

FetchBot: Object Fetching in Cluttered Shelves via Zero-Shot Sim2Real

Weiheng Liu^{1,3,4*} Yuxuan Wan^{2,3*} Jilong Wang^{2,3} Yuxuan Kuang² Xuesong Shi³

Haoran Li¹ Dongbin Zhao¹ Zhizheng Zhang^{3,4†} He Wang^{2,3,4†}

¹ Institute of Automation, Chinese Academy of Sciences ²CFCS, School of Computer Science, Peking University

³Galbot ⁴Beijing Academy of Artificial Intelligence

<https://pku-epic.github.io/FetchBot/>

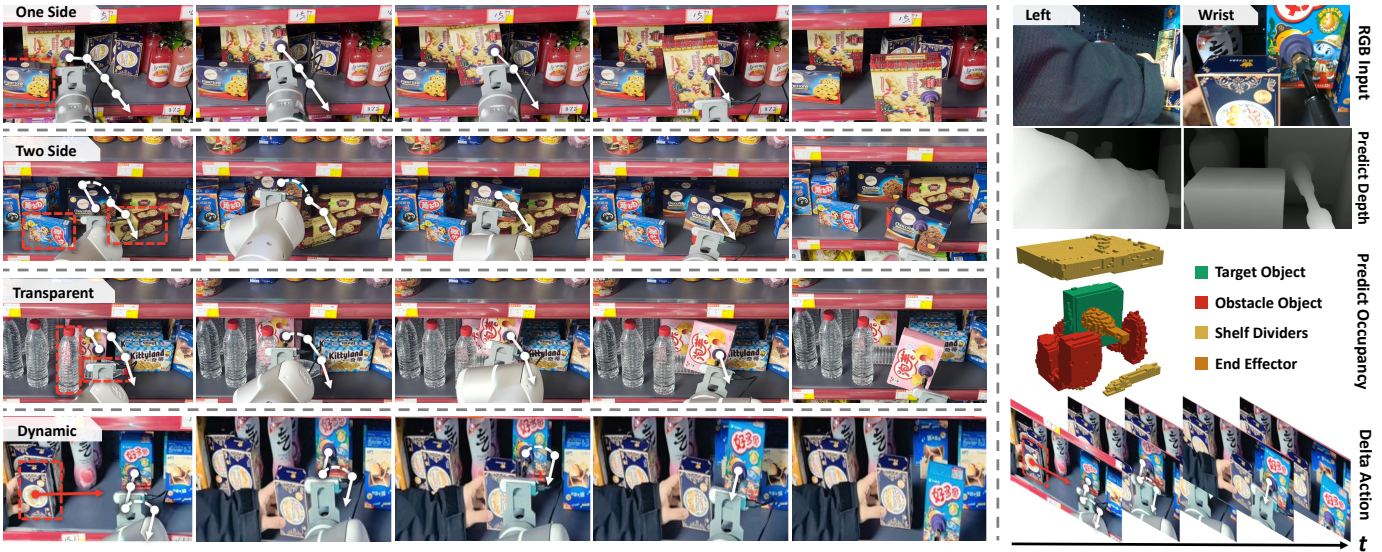


Fig. 1: **FetchBot** is capable of handling a variety of real-world shelf scenarios, including obstacles on one side, obstacles on both sides, transparent obstacles, and dynamic environments.

Abstract—Object fetching from cluttered shelves is an important capability for robots to assist humans in real-world scenarios. Achieving this task demands robotic behaviors that prioritize safety by minimizing disturbances to surrounding objects—an essential but highly challenging requirement due to restricted motion space, limited fields of view, and complex object dynamics. In this paper, we introduce FetchBot, a sim-to-real framework designed to enable zero-shot generalizable and safety-aware object fetching from cluttered shelves in real-world settings. To address data scarcity, we propose an efficient voxel-based method for generating diverse simulated cluttered shelf scenes at scale and train a dynamics-aware reinforcement learning (RL) policy to generate object fetching trajectories within these scenes. This RL policy, which leverages oracle information, is subsequently distilled into a vision-based policy for real-world deployment. Considering that sim-to-real discrepancies stem from texture variations mostly while from geometric dimensions rarely, we propose to adopt depth information estimated by full-fledged depth foundation models as the input for the vision-based policy to mitigate sim-to-real gap. To tackle the challenge of limited views, we design a novel architecture for learning multi-view representations, allowing for comprehensive encoding of cluttered shelf scenes. This enables FetchBot to effectively

minimize collisions while fetching objects from varying positions and depths, ensuring robust and safety-aware operation. Both simulation and real-robot experiments demonstrate FetchBot’s superior generalization ability, particularly in handling a broad range of real-world scenarios, including diverse scene layouts and objects with varying geometries and dimensions.

I. INTRODUCTION

Cluttered shelves are ubiquitous, especially in warehouses, retail stores, libraries and homes, *etc*, making object retrieval a crucial capability for robots assisting humans in diverse scenarios. Fetching objects from cluttered shelves falls under grasping in structured clutter [1], which requires avoiding collisions between the robot, the manipulated objects, and surrounding items. This means that the robot needs to minimize the change of scene structures when it approaches and retrieves the target object from cluttered shelves. Failing to do so could result in undesirable consequences, such as causing nearby objects (especially fragile ones like glass cups) to topple or fall off the shelf. Although robotic fetching has been extensively studied, covering areas such as grasp point detection [2, 3, 4], benchmark development [5], non-prehensile manipulation [6], and mobile manipulation [7, 8], these works

* Core contributors with equal contributions. † Corresponding authors (e-mail: zhangzz@galbot.com, hewang@pku.edu.cn).

have largely overlooked safety concerns during the extraction process. Ensuring robust and safe object fetching in various real-world scenarios remains a challenge, especially in the presence of restricted motion space, limited fields of view, or complex object dynamics.

In this paper, we focus on developing object fetching in cluttered shelves and advancing it to a level of generalization sufficient for real-world applications, as shown in Fig. 1. However, directly training robots in the real world presents challenges such as labor-intensive data collection, safety risks, and scalability issues. Due to the scarcity of real-world data, models trained on such data struggle to achieve the level of generalization required for practical applications, especially when objects on shelves are diverse and their arrangements vary significantly. We emphasize that training with synthetic data offers a promising and cost-effective solution, yet it has been underestimated in the past. To fully leverage the potential of synthetic data, we propose **FetchBot**, a sim-to-real framework designed to enable zero-shot generalizable and safety-aware object fetching from cluttered shelves in real-world settings.

The quality and quantity of data dominate the generalization capacity of learned skills. Although FetchBench [5] introduces a simulation benchmark for robot fetching, the generated scenes are not realistic and diverse enough to bridge the sim-to-real gap for real-world deployment. This is primarily due to excessive spacing between objects, resulting in low item density in their simulated scenes. To address the data scarcity issue, we propose an efficient voxel-based method, Unified Voxel-Based Scene Generator (**UniVoxGen**), for generating diverse and realistic cluttered shelf scenes at scale. UniVoxGen performs collision checking efficiently among objects in the voxel space. In contrast to traditional scene generation methods [9, 10, 11, 5, 12, 13], whose asset loading and collision checking are quite time-consuming, UniVoxGen significantly accelerates the generation process via voxel-based scene representation. Additionally, UniVoxGen can generate realistic shelf layouts by applying a set of carefully hand-designed rules. Beyond efficient large-scale scene generation, we also incorporate a RL-based approach to generate expert trajectories in the generated scenes. Compared to motion planning-based trajectory generation [11], reinforcement learning enables dynamics awareness through extensive feedback from interactions with the environment. This offers an effective method to minimize the collisions between the robot, the manipulated objects, and surrounding items during large-scale synthetic data generation.

To obtain a policy suitable for real-world deployment, we distill these expert trajectories into a closed-loop, vision-based policy through imitation learning. We then explore how to close the sim-to-real gaps. Firstly, we leverage simulation to improve the diversity of synthetic data through extensive randomization of the object to be retrieved, surrounding items, and their layouts. In this way, we enable the training datasets to reach a high diversity efficiently that real-world collected datasets are hard to be comparable. In fact, the sim-to-real

gaps primarily exist in the texture dimension while rarely lie in geometry and material dimensions. Collision avoidance in object fetching relies more on geometry information than on textural information. Thus, secondly, we introduce two novel designs to reduce the reliance on textural information and exploit full-fledged foundation models to reduce the sim-to-real gap of the textural information in our proposed method. One is we make full use of multi-view voxel-based representations for the environments as the model inputs. This helps mitigate the limitations of perceptual views in lateral access environments, enables comprehensive 3D scene understanding, and enhances the vision policy’s generalization ability. To facilitate the learning of these representations, we introduce an occupancy prediction task as an auxiliary objective, encouraging the network to preserve essential geometric information in the voxel-based representations. Empirically, we find that predicting local occupancy around the robotic gripper can drive a better trade-off between the efficiency and effectiveness. The other is we employ a depth foundation model to convert the original RGB inputs into their corresponding depths. This is done during the preprocessing stage of the vision-based policy. In this way, the generalizability of depth foundation models across sim-to-real is fully exploited.

We use a suction cup as our tool for its simplicity and effectiveness in fetching objects from cluttered shelves. Extensive experiments are conducted to evaluate our proposed FetchBot in both simulated and real-world environments, where it demonstrates strong generalization, particularly in handling diverse real-world scenarios.

The core contributions of this work can be summarized in the following four aspects:

- We introduce a zero-shot sim-to-real framework for generalizable object fetching from cluttered shelves in real-world scenes. The learned closed-loop policy is dynamics-aware, capable of avoiding collisions, and generalizes to various environments.
- We propose a synthetic data generation pipeline for producing diverse object-fetching trajectories in cluttered scenes at scale, serving as the foundation of the aforementioned sim-to-real framework.
- We design a novel architecture to learn a unified multi-view 3D representation, focusing solely on the region of interest. This approach enhances scene understanding, significantly improves collision avoidance, and boosts generalization across diverse shelf scenarios.
- We study the scaling characteristics of our proposed method and conduct an in-depth analysis of the roles played by different technical components in bridging the sim-to-real gap, providing insights for broader future applications.

II. RELATED WORKS

Large-scale Cluttered Scene Generation. Automatic scene generation has been extensively studied in computer vision and graphics [14, 15, 16, 17, 18, 19, 20, 21, 22]. However, the structured nature of the scenes generated by these

methods makes them unsuitable for object fetching tasks in cluttered scenes. To address this, some studies [23, 24, 25, 26, 27, 28] have employed simple strategies, such as simulating objects dropped from the air to create cluttered layouts. While effective for disorder, these methods often result in unstable and unrealistic scenes. Recent efforts [9, 10, 11, 5, 12, 13] have aimed to generate more realistic cluttered environments. For example, ClutterGen [9] uses reinforcement learning with physics-based rewards to guide scene generation but is limited by its training object set and lacks generalization. Similarly, works [11, 5, 12, 13, 29] such as Neural MP [11], employ procedural scene generation methods to create cluttered scenarios. These approaches typically rely on complex collision detection mechanisms in simulation to verify scene validity, which significantly limits their efficiency. Moreover, they often support only a single scene generation rule, further constraining the diversity of generated scenes. In response, we propose a novel approach that directly performs scene generation and collision detection in voxel space, eliminating the need for traditional simulations and significantly improving efficiency. By incorporating diverse generation rules, we created a large-scale dataset of 1 million cluttered scenes, offering a valuable resource for studying object fetching in cluttered environments.

Robotic Fetching from Cluttered Scenes. Robotic fetching (grasping) has long been recognized as a fundamental challenge in robotic manipulation, drawing extensive research efforts over the years [30]. A cornerstone in this area is picking objects from cluttered scenes [31, 32, 33, 34, 35, 36, 4, 2, 3, 5, 37, 38], with two primary tasks standing out: bin-picking, which involves vertically lifting objects from cluttered bins [31, 32, 33, 34, 35, 36], and shelf-picking, which entails horizontally extracting items from occluded shelves [4, 2, 3, 5]. Many previous studies on shelf-picking [4, 2, 3] have primarily concentrated on grasp point detection, often overlooking the critical retrieval stage. This stage requires minimizing disturbance to surrounding objects, as even slight collisions can cause nearby items to fall or topple others. Recently, Fetchbench [5] has started addressing the challenges of object fetching from shelves, focusing on more complex aspects of shelf-picking. However, the shelf environments in this work do not accurately reflect real-world conditions. Our approach employs a closed-loop vision-based policy to ensure safe retrieval during the fetching process, minimizing the impact on the surrounding environment.

Sim2Real Transfer for 3D Visuomotor Policies. Currently, there are many 3D-based imitation learning policies [39, 40, 41, 42, 43, 44, 45] that utilize 3D observation data to mimic expert actions from demonstrations. However, these methods predominantly rely on real-world data to perform real-robot tasks, failing to fully leverage the potential of simulators. As a result, sim-to-real transfer for 3D visuomotor policies remains an under-explored topic. Most previous works [46, 47, 48, 49] have employed point clouds as representations to achieve sim-to-real, but they still struggle to bridge the sim-to-real gap due to noise and inaccuracies, particularly at object edges and reflective surfaces in real-world point clouds

captured by depth sensors. To further advance the field of sim-to-real research, inspired by approaches in autonomous driving [50, 51, 52], we propose using a unified 3D representation to ensure consistency in multi-view image fusion and minimize the sim-to-real gap. Through this unified representation and other sim-to-real strategies, our method can successfully achieve sim-to-real transfer.

III. PROBLEM FORMULATION

A. Camera-based 3D Semantic Occupancy Prediction

Given a set of images captured from multiple viewpoints, camera-based 3D semantic occupancy prediction aims to generate a semantically annotated voxel grid within the robot's operational workspace. Specifically, we input multi-camera images $I = \{I^1, I^2, \dots, I^N\}$, and the prediction model Θ will output a semantic voxel volume $\mathbf{Y} \in \{v_0, v_1, \dots, v_C\}^{H \times W \times Z}$. Here, N represents the number of camera viewpoints, C denotes the total number of semantic categories in the scene, v_0 signifies an empty voxel and H, W, Z correspond to the height, width, and depth dimensions of the voxel volume, respectively. In this work, we will use camera-based 3D semantic occupancy prediction as a synergy to pre-train our vision encoder.

B. Problem Definition

Our work primarily focuses on ensuring the safety of the extraction process during object fetching. Specifically, in the shelf environment, there is a target object O_{target} , movable obstacles $O_{obstacle}$ that surround the target, and a fixed shelf O_{shelf} . Our goal is to use the suction cup to extract the target object O_{target} while minimizing the impact E on surrounding obstacles $O_{obstacle}$ and avoiding contact with the shelf's barriers O_{shelf} . We need to utilize a closed-loop vision policy π_{vision} that takes real-world observable inputs \mathcal{O} to complete this task. In this work, the inputs include double-view RGB images $I = \{I^1, I^2\}$ and q^{target} , which represents the relative pose of the end-effector with respect to the target point, i.e., $\mathcal{O} = \{I, q^{target}\}$. By feeding the observations into the vision policy π_{vision} , whose vision encoder is trained using a 3D semantic occupancy prediction auxiliary task, the policy outputs an action $a = \{a_{trans}, a_{rot}\}$, where $a_{trans} \in \mathbb{R}^3$ denotes the relative translation, and $a_{rot} \in SO(3)$ represents the relative rotation, expressed using the axis-angle. Through the iterative execution of the *observation-decision-execution* process in a closed-loop manner, the vision policy π_{vision} can enable the target object O_{target} to reach the target point while minimizing the impact E on the surrounding environment as much as possible.

IV. METHOD

A. Overview

To enable safe and generalizable object fetching in cluttered shelves, we propose a novel sim-to-real framework named **FetchBot**, as illustrated in Fig. 2. FetchBot emphasizes training with synthetic data due to its scalability, cost-effectiveness, and reduced risk. Firstly, to tackle data scarcity,

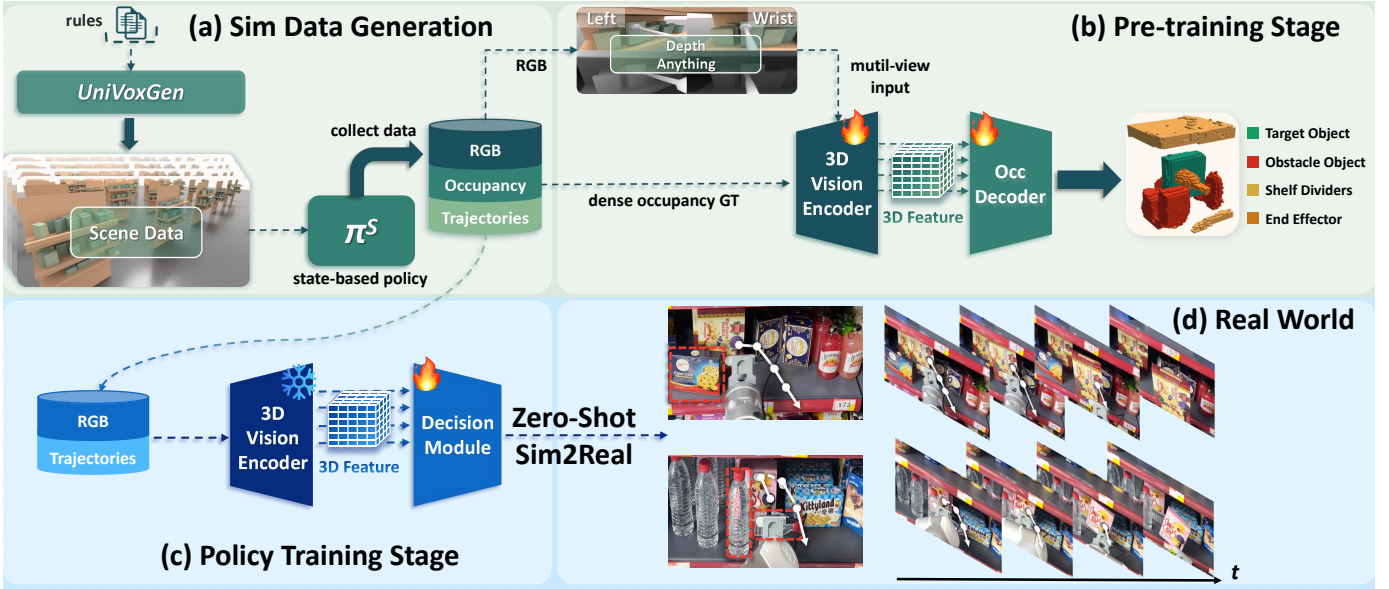


Fig. 2: Our Proposed Framework. In the (a) Sim Data Generation stage, we use UniVoxGen to generate a diverse set of scenes and employ a dynamics-aware RL policy to collect expert trajectories. In the (b) Pre-training stage, we first leverage a foundation model to mitigate the sim-to-real gap, then introduce an occupancy prediction task to learn a voxel-based representation. This task encourages the network to preserve essential geometric information and develop a comprehensive understanding of the scene. In the (c) Policy Training stage, we distill these expert trajectories into a vision-based policy through imitation learning. After training, the vision-based policy can achieve (d) zero-shot sim-to-real.

we introduce **UniVoxGen**, a voxel-based method (Sec. IV-B), which accelerates scene generation by efficiently checking collisions among objects in voxel space and generates realistic scene layouts using several hand-designed rules. Next, to collect trajectories that ensure safety within these generated scenes, we train an RL policy (Sec. IV-C) that leverages oracle information. This policy is dynamics-aware through extensive feedback from interactions with the environment, enabling it to minimize disturbances to surrounding objects. To develop a policy suitable for real-world deployment, we distill these trajectories into a vision-based policy (Sec. IV-D) via imitation learning. To bridge the sim-to-real gap, we use a depth foundation model to generate unified inputs for both simulation and the real world by converting RGB inputs into their corresponding predicted depths. Additionally, we employ multi-view voxel-based representations that focus exclusively on the region of interest, enhancing the policy’s generalization ability and addressing the limitations of narrow views in lateral access environments. By combining the advantages of each component, FetchBot achieves zero-shot sim-to-real transfer and is capable of handling a wide range of real-world scenarios.

B. Voxel-based Cluttered Scene Generator

A diverse and realistic set of scenes is crucial for sim-to-real transfer, requiring an effective scene generation method. Previous works on generating cluttered scenes [23, 24, 25, 26, 27, 28] rely heavily on complex collision detection mechanisms

Algorithm 1 Scene Generation Algorithm

```

Require: Number of scenes  $N$ 
Require: Max objects per scene  $K$ 
Require: A set of objects  $\mathcal{O}$ 
1: for scene  $1 : N$  do
2:   Initialize scene voxel  $V^s = \{\}$ 
3:   Sample a target object  $O^{tar}$ 
4:   Sample a pose  $P$  in  $SE(3)$  for  $O^{tar}$ 
5:   Apply  $T(V_i, P)$  to transform the target object
6:   Apply  $V_{O^{tar}} \cup V^s$  to add the target object to the scene
7:   Sample number of obstacle objects  $k \sim [1, \dots, K]$ 
8:   for obstacle  $O^{obs} 1 : k$  do
9:     Sample a pose  $P$  in  $SE(3)$  for  $O^{obs}$ 
10:    Apply  $T(V_i, P)$  to transform the obstacle object
11:    while  $V_{O^{obs}} \cap V^s$  do
12:      Sample a new pose  $P$  in  $SE(3)$  for  $O^{obs}$ 
13:      Apply  $T(V_i, P)$  to transform the obstacle object
14:    end while
15:    Apply  $V_{O^{obs}} \cup V^s$  to add the obstacle object to the scene
16:  end for
17:  Save the pose  $P$  of each object in the scene
18: end for

```

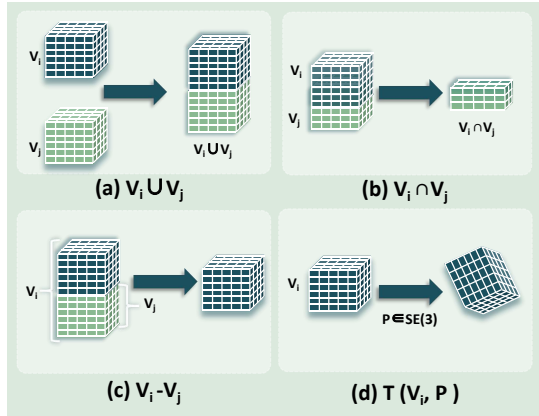


Fig. 3: A set of operational primitives in voxel space.

within simulations to verify the validity of generated scenes, significantly hindering generation efficiency and scalability. Additionally, many of these methods [23, 24, 25, 26, 27, 28] create cluttered layouts by simulating objects dropped from the air, which may result in unstable and unrealistic scene configurations. Our method, **UniVoxGen**, is specifically designed for fast and realistic scene generation in voxel space. It accelerates the generation process by performing efficient collision checks in voxel space and produces realistic scene layouts using a set of carefully crafted hand-designed rules.

We begin by providing formal definitions for key elements in the voxel space. Let $V^o = \{V_1^o, V_2^o, \dots, V_N^o\}$ represent the voxel representation of a set of objects, and $V^s = \{V_1^s, V_2^s, \dots, V_N^s\}$ represent the voxel representation of the scene. As illustrated in Fig. 3, we define a set of operational primitives in voxel space for manipulating voxels. Specifically, $V_i \cup V_j$ denotes the union operation, which combines two voxel sets and is commonly used to add an object's voxels into the scene. $V_i \cap V_j$ denotes the intersection operation, which retrieves the intersection of two voxel sets and is used to detect potential collisions when adding a new object. $V_i - V_j$ denotes the difference operation, which removes the overlapping portion of V_i with V_j , typically used to remove an object from the scene. Finally, $T(V_i, P), P \in SE(3)$ represents a transformation of a voxel V_i in $SE(3)$ space, commonly used to change the pose of the object. Here, P is a transformation matrix in $SE(3)$ that combines rotation and translation.

Based on the previously defined key elements and operation primitives, we further designed a set of generation rules $R = \{R_1, R_2, \dots, R_N\}$. UniVoxGen uses these rules to generate three different levels of cluttered scenes: easy, medium, and hard. Specifically, the easy scene is highly organized, with no obstacles in front of the target object; the medium difficulty scene is partially organized, with a few objects arranged randomly, and there are some obstacles in front of the target object; in the hard difficulty scenes, the obstacles are either highly disordered or tightly attached to the surface of the target object to be fetched. Moreover, these scenes may include

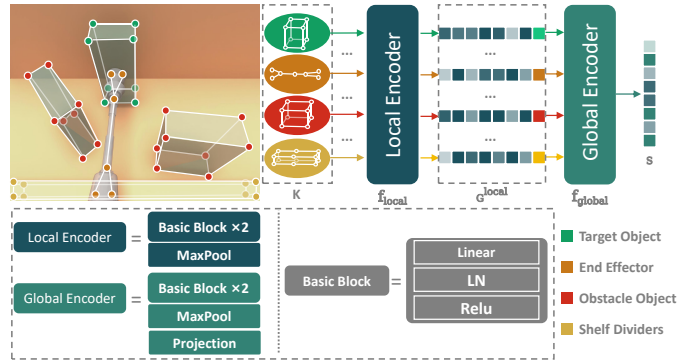


Fig. 4: **Scene Encoder Network in State-Based Policy.** The network follows a hierarchical design. First, a local network is used to extract features specific to the individual objects within the scene. Then, a global network processes these features to capture the overall structure and context of the entire scene.

unsolvable cases, where it is impossible to retrieve the target object without colliding with any obstacles. It is worth noting that the inclusion of unsolvable cases is intended to better simulate real-world scenarios, as such situations can occur in practice. The procedure for generating these cluttered scenes is outlined in Algorithm 1. It should be noted that, given the complexity of the various scene generation rules, the steps presented here represent a simplified version of our scene generation rules. The detailed generation rules will be made available in the subsequently released source code. Finally, we used UniVoxGen to generate 1 million cluttered scenes, which were then utilized as training scene data for a state-based policy. It takes 12 hours on the workstation equipped with 8 RTX 4090s to generate these 1 million scenes, including easy, medium, and hard levels.

C. State-Based Policy

The quality of the demonstrations determines the quality of the distillation. Obtaining expert demonstrations for object fetching from cluttered shelves is challenging, as it requires dynamic awareness to minimize scene disruption. Collision-based motion planning is effective for finding collision-free paths but fails to account for environmental dynamics when such paths are unavailable, which is common in cluttered scenes. This limitation can lead to damaging consequences, such as harming fragile items or destabilizing the scene. Additionally, collision-based approaches tend to be time-consuming, thus reducing data collection efficiency. To address these challenges and inspired by RLDG [53], which shows that RL-generated data achieves better distillation performance than human demonstrations, we adopt a RL policy to collect trajectories. Similar to SafePicking [23], our policy gains dynamic awareness through extensive interaction with the environment, enabling the collection of expert data that minimizes disturbances.

Observations Encoding and Outputs. The observation O_t of the state-based policy π_{state} is defined as:

$$O_t = [q_t^{\text{target}}, a_{t-1}, S_t],$$

where q_t^{target} represents the relative pose of the end-effector with respect to the target goal at time step t , consisting of a rotation matrix rot_t and a translation vector trans_t . The term a_{t-1} denotes the previous action, and S_t is the representation of the scene's geometry, given by:

$$S_t = f_{\text{scene}}(K_t, M_t),$$

where K_t represents the scene's geometry and M_t contains the mask information for each object, indicating whether it is the target, an obstacle, the end effector, or the shelf divider. For simplicity, we will omit the subscript t in the following. As illustrated in Fig. 4, and similar to [54], the scene's geometry K consists of M objects, including the target, obstacles, end-effector, and shelf dividers: $\{K_1, K_2, \dots, K_M\}$, each characterized by a set of N keypoints $\{k_i^1, k_i^2, \dots, k_i^N\}$, uniformly distributed across the object's surface. This flexible representation allows for adaptation to objects with varying geometries and dimensions.

Inspired by PointNet++ [55], we design a hierarchical network f_{scene} that first extracts each object's local geometric features and then derives the global scene feature. Specifically, using f_{local} , we obtain a set of local geometric features $G^{\text{local}} = \{g_1^{\text{local}}, g_2^{\text{local}}, \dots, g_M^{\text{local}}\}$, where $g_i^{\text{local}} = f_{\text{local}}(K_i)$, and f_{local} is a lightweight MLP network with two layers and a max-pooling function for permutation invariance. Next, using f_{global} , which shares the same architecture as f_{local} but includes a projection layer, we obtain the global scene feature:

$$S = f_{\text{global}}(G^{\text{local}}, M),$$

where $M = \{m_1, m_2, \dots, m_M\}$ indicates the object mask information. By concatenating S and M , and passing them through f_{global} , we obtain the final global scene representation. This approach focuses on both the individual objects and the relationships among them, providing a comprehensive scene representation. After feeding the observation O_t into state-based policy π_{state} , it outputs the relative action $a_t = \{a_t^{\text{trans}}, a_t^{\text{rot}}\}$, where $a_t^{\text{trans}} \in \mathbb{R}^3$ denotes the relative translation, and $a_t^{\text{rot}} \in SO(3)$ represents the relative rotation, expressed using the axis-angle.

Reward Functions. The goal of shelf fetching is to minimize the impact on the surrounding environment during both the approach and retrieval processes, thereby avoiding potentially catastrophic consequences. To achieve this, our reward design combines penalties for environmental impact, rewards for task success, and constraints on the actions taken, which can be expressed as:

$$r = \lambda_{\text{impact}} r_{\text{impact}} + \lambda_{\text{task}} r_{\text{task}} + \lambda_{\text{constr}} r_{\text{constr}},$$

where r_{impact} penalizes the impact on surrounding items, in this project, we represent the disturbance to the scene by

using the sum of the translations E_{trans} and the sum of the rotations E_{rot} of all obstacle objects. r_{task} indicates whether the extraction process is successfully completed under the given constraints. In this project, it means that the target object needs to be extracted to the target goal while ensuring that the sum of translations E_{trans} and rotations E_{rot} satisfy: $E_{\text{trans}} < \sigma_{\text{trans}}$ and $E_{\text{rot}} < \sigma_{\text{rot}}$, where σ is scaling term based on the precision requirement. We use a σ curriculum during the training, enabling the successful exploration in the early stages and progressively improving precision in the later stages. r_{constr} represents constraints on the end-effector's behavior, such as limits on angular and linear velocities(see appendix for the details).

D. 3D Vision Policy

To obtain a policy suitable for the real world, we train a vision-based policy using the generated expert trajectories through imitation learning. The goal of object fetching from cluttered shelves is to successfully grasp a target object and move it to a desired location while avoiding collisions with surrounding obstacles. This task is fraught with challenges, the most significant of which is the occlusion of the target object from a single perspective, primarily caused by non-target objects and shelf panels blocking the view. Inspired by advancements in the autonomous driving field [50, 51, 52], our 3D vision policy leverages multi-view inputs to address the issue of limited view fields, and we introduce a camera-based 3D semantic occupancy prediction task as an auxiliary objective, encouraging the network to retain crucial geometric information in voxel-based representations. As shown in Fig. 5, our 3D vision policy consists of two key modules: the perception module and the decision module. (a) The perception module efficiently integrates features from multiple perspectives into a unified voxel-based representation, focusing solely on the region around the robotic gripper. This powerful feature representation provides richer information for decision-making in the subsequent decision module and enhances the model's generalization ability. (b) The decision module processes the output by the perception module using a transformer [56] and employs a high-capacity Diffusion Policy [57] as the core component for action generation.

Perception. As shown in Fig. 5, our 3D vision policy first leverages depth foundation models, such as DepthAnything [58], to convert the raw RGB images I_{RGB} from N camera perspectives into corresponding depth maps I_D . This conversion reduces the sim-to-real gap caused by texture discrepancies in image distributions between the simulated and real environments. Next, we use a backbone network (e.g., ResNet [59]) to extract features $X = \{x_i\}_{i=1}^N$ from these N perspectives, which are then fed into the 3D vision encoder. In the 3D vision encoder, we define a set of learnable local 3D-grid-shaped queries $Q \in \mathbb{R}^{C \times H \times W \times Z}$ centered around the robot's end-effector. Here, H , W , and Z represent the number of cells along the X , Y , and Z axes of the predicted 3D space (in a right-handed coordinate system). For each 3D query, we map it from the 3D space to multiple 2D feature maps F^{2D}

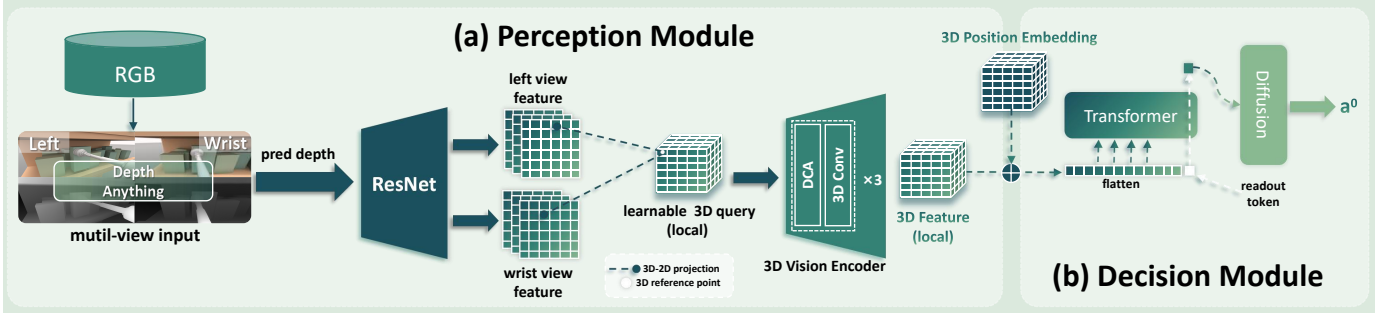


Fig. 5: The **perception module** efficiently integrates features from multiple perspectives into a unified voxel-based representation, focusing solely on the region around the robotic gripper. The **decision module** processes the output by the perception module using a transformer and employs a high-capacity Diffusion Policy as the core component for action generation.

using the given camera intrinsics and extrinsics. Here, we only use the views that the 3D reference point hits. We then apply a deformable cross-attention (DCA) mechanism [60] to sample 2D features around the projected 2D positions:

$$DCA(q_p, F^{2D}) = \frac{1}{|V_{hit}|} \sum_{t \in V_{hit}} DA(q_p, \mathcal{P}(p, t), F_t^{2D}),$$

Here, q_p represents the 3D volume query at point $p = (x, y, z)$, V_{hit} denotes the hit views of the 3D query points, $\mathcal{P}(p, t)$ is the camera projection function, and DA refers to deformable attention. After each DCA operation, we follow the approach from SurroundOcc [52] and apply 3D convolution to further process the sampled 3D features. Finally, in the occupancy prediction stage, we found that predicting occupancy in a smaller local 3D region around the robot's end-effector yields better results compared to predicting the entire shelf's occupancy. This approach not only accelerates the policy inference speed but also enhances generalization performance, as the shape of the obstacles becomes irregular after cropping, making the network more robust.

Decision. In a manner consistent with prior transformer-based policies [61, 62, 63], the decision module leverages a transformer architecture to process the 3D features F^{3D} derived from the perception module. Initially, we augment the 3D features with learnable 3D position embeddings $P^{3D} \in \mathbb{R}^{C \times H \times W \times Z}$. The combined 3D feature map is then flattened, transforming it into a set of 3D feature vectors $V^{3D} \in \mathbb{R}^C$. Then, similar to works such as Octo [61], we use a learnable readout token to query the action features F_A . Finally, we utilize a lightweight diffusion head to progressively denoise random Gaussian noise a^K into the noise-free action a^0 , conditioned on the action features F_A .

Training. Our 3D vision policy is a multi-stage training network. In the first stage, we pre-train the perception module on a large-scale scene dataset using the camera-based 3D semantic occupancy prediction task to achieve comprehensive 3D scene understanding. In the second stage, we freeze the perception module and only train the decision module.

During the first stage, for the occupancy prediction task, the dense occupancy ground truth data is generated using

UniVoxGen. We use the cross-entropy loss and scene-class affinity loss introduced in [51] as supervision signals. In the second stage, we apply the mean squared error loss as the supervision signal to predict the noise added to the original action.

V. EXPERIMENTS

A. Setup

Simulation Setup. We train and evaluate our method in IsaacGym and design various scene layouts using our UniVoxGen, which are categorized into three difficulty levels (see appendix VIII-B for the details):

- **Easy:** In this layout, there are no obstacles in front of the target object, making it straightforward to extract the target.
- **Medium:** The target object is partially occluded by obstacles in front, with the occluded area covering less than 50% of the target's surface.
- **Hard:** The occluded area covers more than 50% of the target's surface, and the nearest obstacle is very close to the target, with a gap of less than 5 mm between them.

During the training phase, we abstract both the target object and obstacles as boxes. This simplifies scene generation and policy training while also reducing the Sim2Real gap [64]. It is important to note that this simplification does not affect the generalization ability of our 3D vision policy to different objects. This is because the occupancy prediction focuses on whether each grid point in the 3D voxel space is occupied, rather than the overall geometric shape of the objects. We have verified this approach in real-world experiments. We used approximately 200 different-sized boxes within an 85cm \times 28cm area to generate around 1 million scenes, with the number of boxes per scene ranging from 3 to 12.

Real-world Setup. In the real-world experiments, we use the Feilix Rizon 4S robotic arm. Two cameras, the Intel D435i and Intel D415i, serve as input for our 3D vision policy from different perspectives, with the Intel D435i fixed at the end effector of the robotic arm. We conduct experiments across three difficulty levels—Easy, Medium, and Hard—on a total of about 30 different scenes and 40 different retail items. Detailed

experimental results can be found in Table. VI. The proposed 3D vision policy exhibited real-time operational performance, achieving a consistent inference rate of 10+ frames per second (fps) on an NVIDIA GeForce RTX 4090 GPU.

B. Implementation details

Our state-based policy is trained on 1 million cluttered scenes, with an equal distribution of easy, medium, and hard scenes (1:1:1 ratio). We then collect approximately 100k expert trajectories for imitation learning.

The proposed 3D vision policy was developed through a two-stage training paradigm utilizing 24 NVIDIA GeForce RTX 4090 GPUs. During the initial stage, the perception module undergoes pretraining on a camera-based 3D semantic occupancy prediction task, consuming approximately 500,000 annotated scenes over 50 training epochs. The architecture incorporates dual visual perspectives: an ego-centric perspective from the robotic wrist-mounted camera and an exocentric observer perspective spatially separated from the robotic arm. During the occupancy prediction, we achieve a spatial resolution of 0.5 cm per voxel. In the subsequent stage, we freeze the pretrained perceptual representations and focus on training the decision module using 100,000 expert demonstration trajectories (comprising 500,000 state-action pairs) across 100 optimization epochs. For systematic evaluation, both baseline methods and our proposed policy undergo rigorous testing on a curated dataset of 3,000 previously unseen scenarios, maintaining an equal distribution across difficulty levels (Easy/Medium/Hard) consistent with training protocols.

C. Baselines and Evaluation Metrics

Baselines. We use the following methods as comparison baselines for our 3D vision policy:

- *Oracle*: This refers to the state-based policy trained using privileged information.
- *Heuristic*: As a simple method for object extraction, the heuristic motion first lifts the target object by the height of the front barrier. Then, it directly extracts the object horizontally.
- *Collision-based motion planning*: We use CuRobo [65] and AIT* [66] as the collision-based motion planning methods. The collision-based approach works well when a collision-free path exists. However, in cluttered scenarios, such as when obstacles are in close contact with the target or when only collisions enable extraction, it struggles to find a safe path.
- *Learning-based method*: We use Vanilla and DP3 [42] as learning-based methods baseline. Vanilla is a simplified version of our 3D vision policy. In this approach, the depth map predicted by DepthAnything is directly fed into a ResNet network to extract features, which are then passed to the Diffusion Policy for action prediction. In the single-view setup, only the wrist perspective is used, while in the double-view setup, both the wrist and third-person perspectives are utilized.

Metrics. In our evaluation process, we utilize various metrics to gauge the quality of our results. We need to consider both the task completion (i.e., whether the target O_{target} is successfully retrieved to the target goal) and the impact E on obstacles $O_{obstacle}$. Therefore, we design two types of metrics:

- E_{trans} and E_{rot} : E_{trans} and E_{rot} represent the total displacement and rotation of obstacles in the environment, respectively.
- *Success Rate*: Success rate (SR) indicates whether the target object can be successfully retrieved to the target goal, while satisfying certain constraints. In this work, we define the constraint as the total displacement of surrounding obstacles not exceeding 3 cm.

It is important to note that due to the challenges of accurately measuring translation error (E_{trans}) and rotation error (E_{rot}) in real-world environments, we use only the success rate as the evaluation metric in the real-world experiments.

D. Main Results

As shown in Table. I, we evaluated the performance of our method against several baselines, including oracle, heuristic, collision-based motion planning, and learning-based approaches such as DP3 and Vanilla. Our method consistently outperforms the baselines (except the oracle, which is our state-based policy) across all difficulty levels (Easy, Medium, and Hard) in terms of success rate (SR), translation error (E_{trans}), and rotation error (E_{rot}). Specifically, our method achieves the highest average SR of 81.46%, significantly outperforming both Vanilla and DP3, particularly in harder scenarios. While the oracle achieves near-perfect performance, it relies on privileged information, making it less applicable to real-world scenarios. Heuristic, although effective in simpler environments, shows a sharp decline in performance as scene complexity increases. Among the collision-based motion planning methods, CuRobo and AIT* demonstrated commendable performance in Easy and Medium scenarios, but both experienced a sharp decline in Hard scenarios. This is primarily because collision-based motion planning methods tend to fail in the presence of collisions, as they often encounter unsolvable situations leading to planning failures. Among the learning-based vision approaches, DP3 performs reasonably well but still falls short compared to our method, especially in handling more complex scenes with occlusion and tight object arrangements. Overall, our approach achieves high success rates and low error metrics, demonstrating superior robustness and generalization across varying levels of difficulty.

E. Ablation Study

Ablation Study on Region of Interest (ROI) Size. Focusing solely on the region of interest is an effective approach that enhances the policy’s generalization ability and aids policy learning. In the ablation study on the Region of Interest (ROI) size (Table. II), we investigate the impact of varying ROI sizes on policy performance. The results show that smaller ROIs, such as $20 \times 20 \times 30$, lead to the best performance, achieving the highest success rate (81.46%) and the lowest translation

Scene Level	Easy			Medium			Hard			Avg.		
Method	SR (%)↑	E_{trans} (cm) ↓	E_{rot} (rad) ↓	SR (%)↑	E_{trans} (cm) ↓	E_{rot} (rad) ↓	SR (%)↑	E_{trans} (cm) ↓	E_{rot} (rad) ↓	SR (%)↑	E_{trans} (cm) ↓	E_{rot} (rad) ↓
Oracle	99.72%	0.17	0.03	90.30%	0.17	0.25	66.79%	4.08	0.59	85.60%	1.47	0.29
Heuristic	100.00%	0.00	0.00	51.03%	6.01	0.94	13.91%	14.13	1.77	54.98%	6.71	0.91
CuRobo	98.95%	0.31	0.05	73.55%	4.56	0.54	32.28%	11.03	1.31	68.26%	3.96	0.63
AIT*	95.46%	0.44	0.07	65.39%	5.51	0.79	26.72%	11.62	1.39	62.52%	5.86	0.75
DP3	92.51%	1.35	0.08	77.80%	4.20	0.48	46.80%	7.94	1.07	72.37%	4.49	0.54
Vanilla (Single View)	87.90%	2.54	0.19	68.40%	5.76	0.73	29.34%	11.22	1.37	61.88%	6.51	0.76
Vanilla (Double View)	89.30%	2.15	0.18	67.88%	5.49	0.67	23.83%	12.08	1.42	60.33%	6.57	0.75
Ours	96.45%	0.87	0.08	86.31%	2.35	0.33	61.63%	5.12	0.72	81.46%	2.78	0.36

TABLE I: Compares the performance of different methods across three difficulty levels (Easy, Medium, Hard) in terms of Success Rate (SR), translation error (E_{trans}), and rotation error (E_{rot}). Our method outperforms all baselines (except for oracle), achieving the highest success rate and the lowest errors in translation and rotation.

ROI Size (cm)	Success Rate (%) ↑	E_{trans} (cm) ↓	E_{rot} (rad) ↓
20 × 20 × 30	81.46%	2.78	0.36
40 × 80 × 30	76.93%	3.24	0.43
60 × 150 × 30	74.63%	3.67	0.47

TABLE II: Ablation study on Region of Interest (ROI) size shows that the smallest ROI (20×20×30 cm) achieves the best results, with the highest success rate and lowest errors. Larger ROIs decrease performance due to irrelevant information from distant areas, highlighting the benefit of smaller, localized ROIs for improved accuracy and efficiency.

Representation	Success Rate (%) ↑	E_{trans} (cm) ↓	E_{rot} (rad) ↓
Oracle	85.77%	0.95	0.02
Point Cloud	71.70%	4.54	0.55
RGB	70.35%	4.97	0.58
Depth	71.44%	4.49	0.56
Pred Depth	61.21%	6.54	0.76
Ours	81.46%	2.78	0.36

TABLE V: Ablation on 3D representations. We replace the visual observation and the corresponding encoder in our 3D vision policy to evaluate different 3D representations.

(2.78 cm) and rotation (0.36 rad) errors. As the ROI size increases, both the success rate and accuracy metrics decrease, with larger ROIs introducing more irrelevant information from distant areas of the scene, which in turn reduces the model’s ability to focus on the target region and make less precise predictions. These findings highlight the advantage of using small, localized ROIs, which not only improve policy performance but also enhance generalization performance, making the network more robust to scene variations. This approach also accelerates policy inference while maintaining high policy performance, especially in cluttered environments.

Dataset Size	Success Rate (%) ↑	E_{trans} (cm) ↓	E_{rot} (rad) ↓
500	62.33%	6.94	0.75
5,000	70.72%	5.08	0.55
50,000	72.50%	4.57	0.51
500,000	81.46%	2.78	0.36
w/o pre-train	77.90%	3.59	0.42

TABLE III: Scaling the training data for occupancy pre-train while maintaining policy training data size.

Ablation Study on Scaling the Training Data. In our ablation study on scaling the training data, we examine its

impact on both the occupancy pre-training (Table. III) and the policy training (Table. IV). For occupancy pre-training, we find a clear correlation between larger datasets and improved performance in policy performance. Starting with 500 scenes, the success rate is 62.33%, accompanied by relatively high translation (6.94 cm) and rotation (0.75 rad) errors. As the dataset size increases to 5,000 and 50k, the success rate improves to 70.72% and 72.50%, respectively, with corresponding reductions in translation and rotation errors. The largest dataset, with 500k scenes, achieves the best performance, reaching a success rate of 81.46% and reducing translation and rotation errors to 2.78 cm and 0.36 rad, respectively. This demonstrates that pre-training on larger datasets significantly enhances the policy performance, providing a more comprehensive understanding of the 3D scene.

Similarly, in the policy training ablation study, we observe a similar trend. With a dataset of 500 state-action pairs, the success rate is 48.23%, with higher translation (9.42 cm) and rotation (1.07 rad) errors. As the dataset increases to 5,000 and 50k, the success rate rises to 54.66% and 65.55%, respectively, with reductions in translation and rotation errors. The largest dataset of 500k state-action pairs yields the best performance, achieving a success rate of 81.46% and reducing translation and rotation errors to 2.78 cm and 0.36 rad. These results highlight that increasing the training data size for the decision module significantly improves task success and reduces errors, emphasizing the importance of a sufficiently large dataset for accurate and reliable policy performance.

Overall, our findings highlight the critical role of large-scale data in both occupancy pre-training and policy training, underscoring the importance of scaling the dataset for improving the overall performance and accuracy of the 3D vision policy.

Dataset Size	Success Rate (%) ↑	E_{trans} (cm) ↓	E_{rot} (rad) ↓
500	48.23%	9.42	1.07
5,000	54.66%	7.99	0.88
50,000	65.55%	4.67	0.62
500,000	81.46%	2.78	0.36

TABLE IV: Scaling the training data for policy while maintaining occupancy pre-training data size.

Method	Easy	Medium	Hard
Heuristic	10/10	2/10	0/10
Ours	10/10	8/10	6/10

TABLE VI: Success Rate in Real-word

Ablation Study on 3D representations. In our ablation study on different 3D representations (in Table. V), we compare the performance of the 3D vision policy using various input types: oracle, point cloud, RGB, depth, predicted depth, and our proposed occupancy prediction. The oracle representation, which utilizes privileged information, achieves the best performance, with a success rate of 85.77% and the lowest translation (0.95 cm) and rotation (0.02 rad) errors. Among the non-privileged representations, point cloud input yields a success rate of 71.70%, while RGB and raw depth inputs show similar performance, with success rates of 70.35% and 71.44%, respectively. Predicted depth, derived from DepthAnything [58], performs the worst with a success rate of 61.21%, suggesting that relying solely on predicted depth data reduces accuracy.

RGB, depth, and predicted depth all use the same multi-view input setup as our occupancy prediction method, which includes both a wrist perspective and a third-person view. However, the feature fusion strategy used for these inputs—simply concatenating features along the channel dimension—fails to fully exploit the rich 3D information available from multiple views. This simplistic fusion approach does not adequately capture the spatial relationships and depth cues crucial for accurate scene understanding. In contrast, our occupancy prediction method leverages a more sophisticated approach to integrate the spatial relationships across views, making full use of the multi-view information. This allows our model to more effectively extract and combine the 3D context, leading to significantly improved performance with a success rate of 81.46%, and lower translation (2.78 cm) and rotation (0.36 rad) errors.

These results highlight the importance of a more nuanced feature fusion strategy and demonstrate that occupancy prediction provides a more robust and accurate representation. By effectively utilizing all available 3D information, our method significantly outperforms the alternatives in guiding the policy.

F. Evaluate in Real-world

As shown in Table. VI, we compare the performance of our method against a heuristic approach across three difficulty levels: Easy, Medium, and Hard. The heuristic method achieves perfect success in the Easy scenario (10/10), but its performance deteriorates significantly in the Medium (2/10) and Hard (0/10) scenarios, where it struggles with partial and full occlusions. In contrast, our method demonstrates robust performance across all difficulty levels, achieving a success rate of 10/10 in the Easy scenario, 8/10 in the Medium scenario, and 6/10 in the Hard scenario. These results highlight that our 3D vision policy, which leverages occupancy

prediction, consistently outperforms the heuristic approach, particularly in more challenging, occluded environments. This underscores the effectiveness and generalization capability of our method, making it a more reliable solution for object extraction tasks in real-world, cluttered scenarios.

VI. LIMITATIONS

Despite the promising results, FetchBot exhibits several limitations that warrant further investigation. First, the reliance on a suction-based grasping mechanism introduces constraints related to object surface characteristics and weight. Specifically, the system may experience suction failure when encountering irregular or uneven surfaces, and gravitational forces may cause detachment when manipulating objects exceeding the suction cup’s weight capacity. Second, while the integration of DepthAnything [58] has enhanced the model’s generalization capabilities, the system’s overall performance remains inherently bounded by the limitations of the DepthAnything framework itself. Third, the current implementation employs a spatial resolution of 0.5 cm per voxel for occupancy prediction, which, while sufficient for many scenarios, proves inadequate in highly complex and highly dynamic changing environments. Although increasing the spatial resolution could potentially address this limitation, such enhancement would necessitate significantly greater computational resources, presenting a critical trade-off between precision and computational efficiency that merits further exploration in future work.

VII. CONCLUSIONS

This paper introduces **FetchBot**, a sim-to-real framework designed for safe object fetching in densely cluttered shelves. By integrating large-scale synthetic data generation, dynamics-aware policy learning, and unified multi-view 3D representations, FetchBot achieves zero-shot generalization to real-world scenarios with minimal disturbance to surrounding objects. Specifically, we propose **UniVoxGen** to overcome data scarcity by generating high-density, geometrically diverse scene layouts in voxel space, enabling state-based policy training. Through oracle-guided trajectory distillation and integration with depth foundation models, FetchBot mitigates sim-to-real discrepancies while preserving geometric fidelity for collision avoidance. The architecture of our 3D vision policy focuses on local occupancy prediction and view-consistent 3D scene understanding significantly improves performance in restricted motion spaces and occluded views. In simulation, FetchBot outperforms motion planning and state-of-the-art learning-based methods, achieving an average success rate of 81.46%. In real-world experiments, it demonstrates a 76.67% success rate across 30 diverse retail scenarios with over 40+ distinct retail items. These results highlight the viability of simulation-driven approaches augmented with foundation models and geometry-aware representations for developing safe, efficient, and generalizable robotic systems. Future work will explore non-suction manipulation and more complex shelf dynamic environments to further bridge the gap between simulation and real-world deployment.

REFERENCES

- [1] Jens Lundell, Francesco Verdoja, and Ville Kyrki. Ddgc: Generative deep dexterous grasping in clutter. *IEEE Robotics and Automation Letters*, 6(4):6899–6906, 2021.
- [2] Boling Yang, Soofiyan Atar, Markus Grotz, Byron Boots, and Joshua Smith. Dynamo-grasp: Dynamics-aware optimization for grasp point detection in suction grippers. In *Conference on Robot Learning*, pages 2096–2112. PMLR, 2023.
- [3] Soofiyan Atar, Yi Li, Markus Grotz, Michael Wolf, Dieter Fox, and Joshua Smith. Optigrasp: Optimized grasp pose detection using rgb images for warehouse picking robots. *arXiv preprint arXiv:2409.19494*, 2024.
- [4] Michael Murray, Abhishek Gupta, and Maya Cakmak. Learning to grasp in clutter with interactive visual failure prediction. In *2024 IEEE International Conference on Robotics and Automation (ICRA)*, pages 18172–18178. IEEE, 2024.
- [5] Beining Han, Meenal Parakh, Derek Geng, Jack A Defay, Gan Luyang, and Jia Deng. Fetchbench: A simulation benchmark for robot fetching. *arXiv preprint arXiv:2406.11793*, 2024.
- [6] Albert Wu and Dan Kruse. In the wild ungraspable object picking with bimanual nonprehensile manipulation. *arXiv preprint arXiv:2409.15465*, 2024.
- [7] Max Bajracharya, James Borders, Richard Cheng, Dan Helmick, Lukas Kaul, Dan Kruse, John Leichty, Jeremy Ma, Carolyn Matl, Frank Michel, et al. Demonstrating mobile manipulation in the wild: A metrics-driven approach. *arXiv preprint arXiv:2401.01474*, 2024.
- [8] Max Spahn, Corrado Pezzato, Chadi Salmi, Rick Dekker, Cong Wang, Christian Pek, Jens Kober, Javier Alonso-Mora, C Hernandez Corbato, and Martijn Wisse. Demonstrating adaptive mobile manipulation in retail environments. *Proceedings of the Robotics: Science and System XX*, 2024.
- [9] Yinsen Jia and Boyuan Chen. Cluttergen: A cluttered scene generator for robot learning. In *8th Annual Conference on Robot Learning*, 2024.
- [10] Mengqi Zhou, Yuxi Wang, Jun Hou, Chuanchen Luo, Zhaoxiang Zhang, and Junran Peng. Scenex: Procedural controllable large-scale scene generation via large-language models. *arXiv preprint arXiv:2403.15698*, 2024.
- [11] Murtaza Dalal, Jiahui Yang, Russell Mendonca, Youssef Khaky, Ruslan Salakhutdinov, and Deepak Pathak. Neural mp: A generalist neural motion planner. *arXiv preprint arXiv:2409.05864*, 2024.
- [12] Adithyavairavan Murali, Arsalan Mousavian, Clemens Eppner, Adam Fishman, and Dieter Fox. Cabinet: Scaling neural collision detection for object rearrangement with procedural scene generation. In *2023 IEEE International Conference on Robotics and Automation (ICRA)*, pages 1866–1874. IEEE, 2023.
- [13] Constantinos Chamzas, Carlos Quintero-Pena, Zachary Kingston, Andreas Orthey, Daniel Rakita, Michael Gleicher, Marc Toussaint, and Lydia E Kavraki. Motion-benchmarker: A tool to generate and benchmark motion planning datasets. *IEEE Robotics and Automation Letters*, 7(2):882–889, 2021.
- [14] Xinpeng Wang, Chandan Yeshwanth, and Matthias Nießner. Sceneformer: Indoor scene generation with transformers. In *2021 International Conference on 3D Vision (3DV)*, pages 106–115. IEEE, 2021.
- [15] Angel Chang, Will Monroe, Manolis Savva, Christopher Potts, and Christopher D Manning. Text to 3d scene generation with rich lexical grounding. *arXiv preprint arXiv:1505.06289*, 2015.
- [16] Angel Chang, Manolis Savva, and Christopher D Manning. Learning spatial knowledge for text to 3d scene generation. In *Proceedings of the 2014 conference on empirical methods in natural language processing (EMNLP)*, pages 2028–2038, 2014.
- [17] Daniel Ritchie, Kai Wang, and Yu-an Lin. Fast and flexible indoor scene synthesis via deep convolutional generative models. In *Proceedings of the IEEE/CVF Conference on Computer Vision and Pattern Recognition*, pages 6182–6190, 2019.
- [18] Despoina Paschalidou, Amlan Kar, Maria Shugrina, Karsten Kreis, Andreas Geiger, and Sanja Fidler. Atiss: Autoregressive transformers for indoor scene synthesis. *Advances in Neural Information Processing Systems*, 34:12013–12026, 2021.
- [19] Wamiq Reyaz Para, Paul Guerrero, Niloy Mitra, and Peter Wonka. Cofs: Controllable furniture layout synthesis. In *ACM SIGGRAPH 2023 Conference Proceedings*, pages 1–11, 2023.
- [20] Weixi Feng, Wanrong Zhu, Tsu-jui Fu, Varun Jampani, Arjun Akula, Xuehai He, Sugato Basu, Xin Eric Wang, and William Yang Wang. Layoutgpt: Compositional visual planning and generation with large language models. *Advances in Neural Information Processing Systems*, 36, 2024.
- [21] Miguel Angel Bautista, Pengsheng Guo, Samira Abnar, Walter Talbott, Alexander Toshev, Zhuoyuan Chen, Laurent Dinh, Shuangfei Zhai, Hanlin Goh, Daniel Ulbricht, et al. Gaudi: A neural architect for immersive 3d scene generation. *Advances in Neural Information Processing Systems*, 35:25102–25116, 2022.
- [22] Huan Fu, Bowen Cai, Lin Gao, Ling-Xiao Zhang, Jiaming Wang, Cao Li, Qixun Zeng, Chengyue Sun, Rongfei Jia, Binqiang Zhao, et al. 3d-front: 3d furnished rooms with layouts and semantics. In *Proceedings of the IEEE/CVF International Conference on Computer Vision*, pages 10933–10942, 2021.
- [23] Kentaro Wada, Stephen James, and Andrew J Davison. Safepicking: Learning safe object extraction via object-level mapping. In *2022 International Conference on Robotics and Automation (ICRA)*, pages 10202–10208. IEEE, 2022.
- [24] Yitong Li, Ruihai Wu, Haoran Lu, Chuanruo Ning,

- Yan Shen, Guanqi Zhan, and Hao Dong. Broadcasting support relations recursively from local dynamics for object retrieval in clutters. In *Robotics: Science and Systems*, 2024.
- [25] Kechun Xu, Shuqi Zhao, Zhongxiang Zhou, Zizhang Li, Huaijin Pi, Yifeng Zhu, Yue Wang, and Rong Xiong. A joint modeling of vision-language-action for target-oriented grasping in clutter. In *2023 IEEE International Conference on Robotics and Automation (ICRA)*, pages 11597–11604. IEEE, 2023.
- [26] Yaoao Qian, Xupeng Zhu, Ondrej Biza, Shuo Jiang, Linfeng Zhao, Haojie Huang, Yu Qi, and Robert Platt. Thinkgrasp: A vision-language system for strategic part grasping in clutter. *arXiv preprint arXiv:2407.11298*, 2024.
- [27] Yuxiang Yang, Jiangtao Guo, Zilong Li, Zhiwei He, and Jing Zhang. Ground4act: Leveraging visual-language model for collaborative pushing and grasping in clutter. *Image and Vision Computing*, 151:105280, 2024.
- [28] Yongliang Wang and Hamidreza Kasaei. Learning dual-arm push and grasp synergy in dense clutter. *arXiv preprint arXiv:2412.04052*, 2024.
- [29] Adam Fishman, Aaron Walsman, Mohak Bhardwaj, Wentao Yuan, Balakumar Sundaralingam, Byron Boots, and Dieter Fox. Avoid everything: Model-free collision avoidance with expert-guided fine-tuning. In *CoRL Workshop on Safe and Robust Robot Learning for Operation in the Real World*, 2024.
- [30] Rhys Newbury, Morris Gu, Lachlan Chumbley, Arsalan Mousavian, Clemens Eppner, Jürgen Leitner, Jeannette Bohg, Antonio Morales, Tamim Asfour, Danica Kragic, et al. Deep learning approaches to grasp synthesis: A review. *IEEE Transactions on Robotics*, 39(5):3994–4015, 2023.
- [31] Nikolaus Correll, Kostas E Bekris, Dmitry Berenson, Oliver Brock, Albert Causo, Kris Hauser, Kei Okada, Alberto Rodriguez, Joseph M Romano, and Peter R Wurman. Analysis and observations from the first amazon picking challenge. *IEEE Transactions on Automation Science and Engineering*, 15(1):172–188, 2016.
- [32] Clemens Eppner, Sebastian Höfer, Rico Jonschkowski, Roberto Martín-Martín, Arne Sieverling, Vincent Wall, and Oliver Brock. Lessons from the amazon picking challenge: Four aspects of building robotic systems. In *Robotics: science and systems*, volume 12, 2016.
- [33] Jeffrey Mahler and Ken Goldberg. Learning deep policies for robot bin picking by simulating robust grasping sequences. In *Conference on robot learning*, pages 515–524. PMLR, 2017.
- [34] Jeffrey Mahler, Matthew Matl, Vishal Satish, Michael Danielczuk, Bill DeRose, Stephen McKinley, and Ken Goldberg. Learning ambidextrous robot grasping policies. *Science Robotics*, 4(26):eaau4984, 2019.
- [35] Kuan-Ting Yu, Nima Fazeli, Nikhil Chavan-Dafle, Orion Taylor, Elliott Donlon, Guillermo Diaz Lankenau, and Alberto Rodriguez. A summary of team mit’s approach to the amazon picking challenge 2015. *arXiv preprint arXiv:1604.03639*, 2016.
- [36] Juncheng Li and David J Cappelleri. Sim-suction: Learning a suction grasp policy for cluttered environments using a synthetic benchmark. *IEEE Transactions on Robotics*, 2023.
- [37] Jiazhao Zhang, Nandiraju Gireesh, Jilong Wang, Xiaomeng Fang, Chaoyi Xu, Weiguang Chen, Liu Dai, and He Wang. Gamma: Graspability-aware mobile manipulation policy learning based on online grasping pose fusion. In *2024 IEEE International Conference on Robotics and Automation (ICRA)*, pages 1399–1405. IEEE, 2024.
- [38] Jilong Wang, Javokhirbek Rajabov, Chaoyi Xu, Yiming Zheng, and He Wang. Quadwbg: Generalizable quadrupedal whole-body grasping. *arXiv preprint arXiv:2411.06782*, 2024.
- [39] Mohit Shridhar, Lucas Manuelli, and Dieter Fox. Perceiver-actor: A multi-task transformer for robotic manipulation. In *Conference on Robot Learning*, pages 785–799. PMLR, 2023.
- [40] Ankit Goyal, Jie Xu, Yijie Guo, Valts Blukis, Yu-Wei Chao, and Dieter Fox. Rvt: Robotic view transformer for 3d object manipulation. In *Conference on Robot Learning*, pages 694–710. PMLR, 2023.
- [41] Theophile Gervet, Zhou Xian, Nikolaos Gkanatsios, and Katerina Fragkiadaki. Act3d: Infinite resolution action detection transformer for robotic manipulation. *arXiv preprint arXiv:2306.17817*, 2023.
- [42] Yanjie Ze, Gu Zhang, Kangning Zhang, Chenyuan Hu, Muhan Wang, and Huazhe Xu. 3d diffusion policy: Generalizable visuomotor policy learning via simple 3d representations. In *ICRA 2024 Workshop on 3D Visual Representations for Robot Manipulation*, 2024.
- [43] Tsung-Wei Ke, Nikolaos Gkanatsios, and Katerina Fragkiadaki. 3d diffuser actor: Policy diffusion with 3d scene representations. *arXiv preprint arXiv:2402.10885*, 2024.
- [44] Zhou Xian, Nikolaos Gkanatsios, Theophile Gervet, Tsung-Wei Ke, and Katerina Fragkiadaki. Chaineddiffuser: Unifying trajectory diffusion and keypose prediction for robotic manipulation. In *7th Annual Conference on Robot Learning*, 2023.
- [45] I Liu, Chun Arthur, Sicheng He, Daniel Seita, and Gaurav Sukhatme. Voxact-b: Voxel-based acting and stabilizing policy for bimanual manipulation. *arXiv preprint arXiv:2407.04152*, 2024.
- [46] Jiangran Lyu, Yuxing Chen, Tao Du, Feng Zhu, Huiquan Liu, Yizhou Wang, and He Wang. Scissorbot: Learning generalizable scissor skill for paper cutting via simulation, imitation, and sim2real. *arXiv preprint arXiv:2409.13966*, 2024.
- [47] Pengwei Xie, Rui Chen, Siang Chen, Yuzhe Qin, Fanbo Xiang, Tianyu Sun, Jing Xu, Guijin Wang, and Hao Su. Part-guided 3d rl for sim2real articulated object manipulation. *IEEE Robotics and Automation Letters*, 2023.

- [48] Yuzhe Qin, Binghao Huang, Zhao-Heng Yin, Hao Su, and Xiaolong Wang. Dexpoint: Generalizable point cloud reinforcement learning for sim-to-real dexterous manipulation. In *Conference on Robot Learning*, pages 594–605. PMLR, 2023.
- [49] Zifan Wang, Ziqing Chen, Junyu Chen, Jilong Wang, Yuxin Yang, Yunze Liu, Xueyi Liu, He Wang, and Li Yi. Mobileh2r: Learning generalizable human to mobile robot handover exclusively from scalable and diverse synthetic data. *arXiv preprint arXiv:2501.04595*, 2025.
- [50] Yuqi Wang, Yuntao Chen, Xingyu Liao, Lue Fan, and Zhaoxiang Zhang. Panoocc: Unified occupancy representation for camera-based 3d panoptic segmentation. In *Proceedings of the IEEE/CVF conference on computer vision and pattern recognition*, pages 17158–17168, 2024.
- [51] Anh-Quan Cao and Raoul De Charette. Monoscene: Monocular 3d semantic scene completion. In *Proceedings of the IEEE/CVF Conference on Computer Vision and Pattern Recognition*, pages 3991–4001, 2022.
- [52] Yi Wei, Linqing Zhao, Wenzhao Zheng, Zheng Zhu, Jie Zhou, and Jiwen Lu. Surroundocc: Multi-camera 3d occupancy prediction for autonomous driving. In *Proceedings of the IEEE/CVF International Conference on Computer Vision*, pages 21729–21740, 2023.
- [53] Charles Xu, Qiyang Li, Jianlan Luo, and Sergey Levine. Rldg: Robotic generalist policy distillation via reinforcement learning. *arXiv preprint arXiv:2412.09858*, 2024.
- [54] Haonan Chen, Yilong Niu, Kaiwen Hong, Shuijing Liu, Yixuan Wang, Yunzhu Li, and Katherine Rose Driggs-Campbell. Predicting object interactions with behavior primitives: An application in stowing tasks. In *7th Annual Conference on Robot Learning*, 2023.
- [55] Charles Ruizhongtai Qi, Li Yi, Hao Su, and Leonidas J Guibas. Pointnet++: Deep hierarchical feature learning on point sets in a metric space. *Advances in neural information processing systems*, 30, 2017.
- [56] A Vaswani. Attention is all you need. *Advances in Neural Information Processing Systems*, 2017.
- [57] Cheng Chi, Zhenjia Xu, Siyuan Feng, Eric Cousineau, Yilun Du, Benjamin Burchfiel, Russ Tedrake, and Shuran Song. Diffusion policy: Visuomotor policy learning via action diffusion. *The International Journal of Robotics Research*, page 02783649241273668, 2023.
- [58] Lihe Yang, Bingyi Kang, Zilong Huang, Zhen Zhao, Xiaogang Xu, Jiashi Feng, and Hengshuang Zhao. Depth anything v2. *arXiv preprint arXiv:2406.09414*, 2024.
- [59] Kaiming He, Xiangyu Zhang, Shaoqing Ren, and Jian Sun. Deep residual learning for image recognition. In *Proceedings of the IEEE conference on computer vision and pattern recognition*, pages 770–778, 2016.
- [60] Xizhou Zhu, Weijie Su, Lewei Lu, Bin Li, Xiaogang Wang, and Jifeng Dai. Deformable detr: Deformable transformers for end-to-end object detection. *arXiv preprint arXiv:2010.04159*, 2020.
- [61] Octo Model Team, Dibya Ghosh, Homer Walke, Karl Pertsch, Kevin Black, Oier Mees, Sudeep Dasari, Joey Hejna, Tobias Kreiman, Charles Xu, et al. Octo: An open-source generalist robot policy. *arXiv preprint arXiv:2405.12213*, 2024.
- [62] Moo Jin Kim, Karl Pertsch, Siddharth Karamcheti, Ted Xiao, Ashwin Balakrishna, Suraj Nair, Rafael Rafailov, Ethan Foster, Grace Lam, Pannag Sanketi, Quan Vuong, Thomas Kollar, Benjamin Burchfiel, Russ Tedrake, Dorsa Sadigh, Sergey Levine, Percy Liang, and Chelsea Finn. Openvla: An open-source vision-language-action model. *arXiv preprint arXiv:2406.09246*, 2024.
- [63] Chenxi Wang, Hongjie Fang, Hao-Shu Fang, and Cewu Lu. Rise: 3d perception makes real-world robot imitation simple and effective. *arXiv preprint arXiv:2404.12281*, 2024.
- [64] Tan Zhang, Kefang Zhang, Jiatao Lin, Wing-Yue Geoffrey Louie, and Hui Huang. Sim2real learning of obstacle avoidance for robotic manipulators in uncertain environments. *IEEE Robotics and Automation Letters*, 7(1):65–72, 2021.
- [65] Balakumar Sundaralingam, Siva Kumar Sastry Hari, Adam Fishman, Caelan Garrett, Karl Van Wyk, Valts Blukis, Alexander Millane, Helen Oleynikova, Ankur Handa, Fabio Ramos, et al. Curobo: Parallelized collision-free robot motion generation. In *2023 IEEE International Conference on Robotics and Automation (ICRA)*, pages 8112–8119. IEEE, 2023.
- [66] Marlin P Strub and Jonathan D Gammell. Adaptively informed trees (ait*): Fast asymptotically optimal path planning through adaptive heuristics. In *2020 IEEE International Conference on Robotics and Automation (ICRA)*, pages 3191–3198. IEEE, 2020.
- [67] Yongxing Dai, Jun Liu, Yifan Sun, Zekun Tong, Chi Zhang, and Ling-Yu Duan. Idm: An intermediate domain module for domain adaptive person re-id. In *Proceedings of the IEEE/CVF international conference on computer vision*, pages 11864–11874, 2021.
- [68] Xian Zhao, Lei Huang, Jie Nie, and Zhiqiang Wei. Towards adaptive multi-scale intermediate domain via progressive training for unsupervised domain adaptation. *IEEE Transactions on Multimedia*, 2023.
- [69] Yongxing Dai, Yifan Sun, Jun Liu, Zekun Tong, and Ling-Yu Duan. Bridging the source-to-target gap for cross-domain person re-identification with intermediate domains. *International Journal of Computer Vision*, pages 1–25, 2024.
- [70] Caroline Claus and Craig Boutilier. The dynamics of reinforcement learning in cooperative multiagent systems. *AAAI/IAAI*, 1998(746-752):2, 1998.
- [71] Daan Bloembergen, Karl Tuyls, Daniel Hennes, and Michael Kaisers. Evolutionary dynamics of multi-agent learning: A survey. *Journal of Artificial Intelligence Research*, 53:659–697, 2015.
- [72] Michael Everett, Yu Fan Chen, and Jonathan P How. Motion planning among dynamic, decision-making agents

- with deep reinforcement learning. In *2018 IEEE/RSJ International Conference on Intelligent Robots and Systems (IROS)*, pages 3052–3059. IEEE, 2018.
- [73] John Schulman, Yan Duan, Jonathan Ho, Alex Lee, Ibrahim Awwal, Henry Bradlow, Jia Pan, Sachin Patil, Ken Goldberg, and Pieter Abbeel. Motion planning with sequential convex optimization and convex collision checking. *The International Journal of Robotics Research*, 33(9):1251–1270, 2014.
- [74] Laurene Claussmann, Marc Revilloud, Dominique Gruyer, and Sébastien Glaser. A review of motion planning for highway autonomous driving. *IEEE Transactions on Intelligent Transportation Systems*, 21(5):1826–1848, 2019.
- [75] Zhigen Zhao, Shuo Cheng, Yan Ding, Ziyi Zhou, Shiqi Zhang, Danfei Xu, and Ye Zhao. A survey of optimization-based task and motion planning: From classical to learning approaches. *IEEE/ASME Transactions on Mechatronics*, 2024.
- [76] Clément Godard, Oisin Mac Aodha, Michael Firman, and Gabriel J Brostow. Digging into self-supervised monocular depth estimation. In *Proceedings of the IEEE/CVF international conference on computer vision*, pages 3828–3838, 2019.
- [77] Wenbo Hu, Xiangjun Gao, Xiaoyu Li, Sijie Zhao, Xiaodong Cun, Yong Zhang, Long Quan, and Ying Shan. Depthcrafter: Generating consistent long depth sequences for open-world videos. *arXiv preprint arXiv:2409.02095*, 2024.
- [78] Haotong Lin, Sida Peng, Jingxiao Chen, Songyou Peng, Jiaming Sun, Minghuan Liu, Hujun Bao, Jiashi Feng, Xiaowei Zhou, and Bingyi Kang. Prompting depth anything for 4k resolution accurate metric depth estimation. *arXiv preprint arXiv:2412.14015*, 2024.
- [79] Jiahao Shao, Yuanbo Yang, Hongyu Zhou, Youmin Zhang, Yujun Shen, Matteo Poggi, and Yiyi Liao. Learning temporally consistent video depth from video diffusion priors. *arXiv preprint arXiv:2406.01493*, 2024.
- [80] Nathan Ratliff, Matt Zucker, J Andrew Bagnell, and Siddhartha Srinivasa. Chomp: Gradient optimization techniques for efficient motion planning. In *2009 IEEE international conference on robotics and automation*, pages 489–494. IEEE, 2009.
- [81] Huang Huang, Michael Danielczuk, Chung Min Kim, Letian Fu, Zachary Tam, Jeffrey Ichnowski, Anelia Angelova, Brian Ichter, and Ken Goldberg. Mechanical search on shelves using a novel “bluction” tool. In *2022 International Conference on Robotics and Automation (ICRA)*, pages 6158–6164. IEEE, 2022.
- [82] Ankit Goyal, Valts Blukis, Jie Xu, Yijie Guo, Yu-Wei Chao, and Dieter Fox. Rvt-2: Learning precise manipulation from few demonstrations. *arXiv preprint arXiv:2406.08545*, 2024.
- [83] Yuxuan Wan, Kaichen Zhou, Jinhong Chen, and Hao Dong. Scanet: Correcting lego assembly errors with self-correct assembly network. In *2024 IEEE/RSJ International Conference on Intelligent Robots and Systems (IROS)*, pages 5940–5947. IEEE, 2024.
- [84] Yunlong Tang, Yuxuan Wan, Lei Qi, and Xin Geng. Dpstyler: dynamic promptstyler for source-free domain generalization. *IEEE Transactions on Multimedia*, 2025.
- [85] Kaichen Zhou. Neural surface reconstruction from sparse views using epipolar geometry. *arXiv preprint arXiv:2406.04301*, 2024.

Hyper-parameters	Values
λ_{task}	1.0
λ_{trans_step}	-0.5
λ_{rot_step}	-0.5
λ_{trans_termi}	-1.0
λ_{rot_termi}	-1.0
λ_{vel}	-0.5
λ_{ang}	-0.3
λ_{pose}	-0.1
$\lambda_{penetration}$	-1.0

TABLE VII: Hyper-parameters for the reward function.

Hyper-parameters	Values
Num. envs	1024
Num. steps for per update	24
Num. minibatches	4
Num. learning epochs	1500
learning rate	0.0003
clip range	0.2
entropy coefficient	0.0
kl threshold	0.02
max gradient norm	1.0
λ	0.95
γ	0.99

TABLE VIII: Hyper-parameters for the oracle policy learning.

VIII. APPENDIX

A. Hyper-parameters in State-Based Policy Training

During state-based policy training, our reward function is a combination of $r_{task}, r_{impact}, r_{constr}$.

The robot behavior constrain reward r_{constr} consists of $r_{vel}, r_{ang}, r_{penetration}, r_{pose}$. The r_{vel} and r_{ang} limit the end-effector's linear velocity and rotational velocity to a threshold. $r_{penetration}$ prevents the end-effector and the target object from colliding with the fixed shelf, as such a collision would lead to significant linear and rotational acceleration due to penetration with the shelf. r_{pose} encourages the robot to maintain a kinematically feasible state.

The impact reward r_{impact} consists of $r_{trans_step}, r_{rot_step}, r_{trans_termi}, r_{rot_termi}$. The step rewards $r_{trans_step}, r_{rot_step}$ penalize the actions taken in each step based on the total translation E_{trans} and rotation E_{rot} within that step. The termination rewards $r_{trans_termi}, r_{rot_termi}$ penalize the entire extraction process based on the total translation E_{trans} and rotation E_{rot} over the entire process.

The task reward r_{task} corresponds to successfully fetching the target object, and the total translation E_{trans} and rotation E_{rot} during the entire fetching process must satisfy : $E_{trans} < \sigma_{trans}, E_{rot} < \sigma_{rot}$. We use a σ curriculum to guide the learning process. Once the policy saturates in the current curriculum, we increase the difficulty. Specifically, we set the σ_{trans} to [0.03, 0.015, 0.01, 0.005, 0], and we set σ_{rot} to [0.4, 0.2, 0.16, 0.1, 0].

We combine the above rewards with weights listed in Table VII.

We train our oracle policy with PPO, and the training hyper-parameters are shown in Table VIII.

B. Generated scenes by UniVoxGen

We use six carefully hand-designed rules to generate realistic shelf layouts using UniVoxGen. The scene is divided into three difficulty levels. The following are the generated scenes displayed both in the simulation and voxel space.

C. Items in Real-World Experiments

We used approximately 40 items with various shapes for the real-world experiments, as shown in Figure 9. These items encompass a wide range of objects commonly found in retail environments, including boxed items, bottled objects, bagged goods, and fragile items, among others.

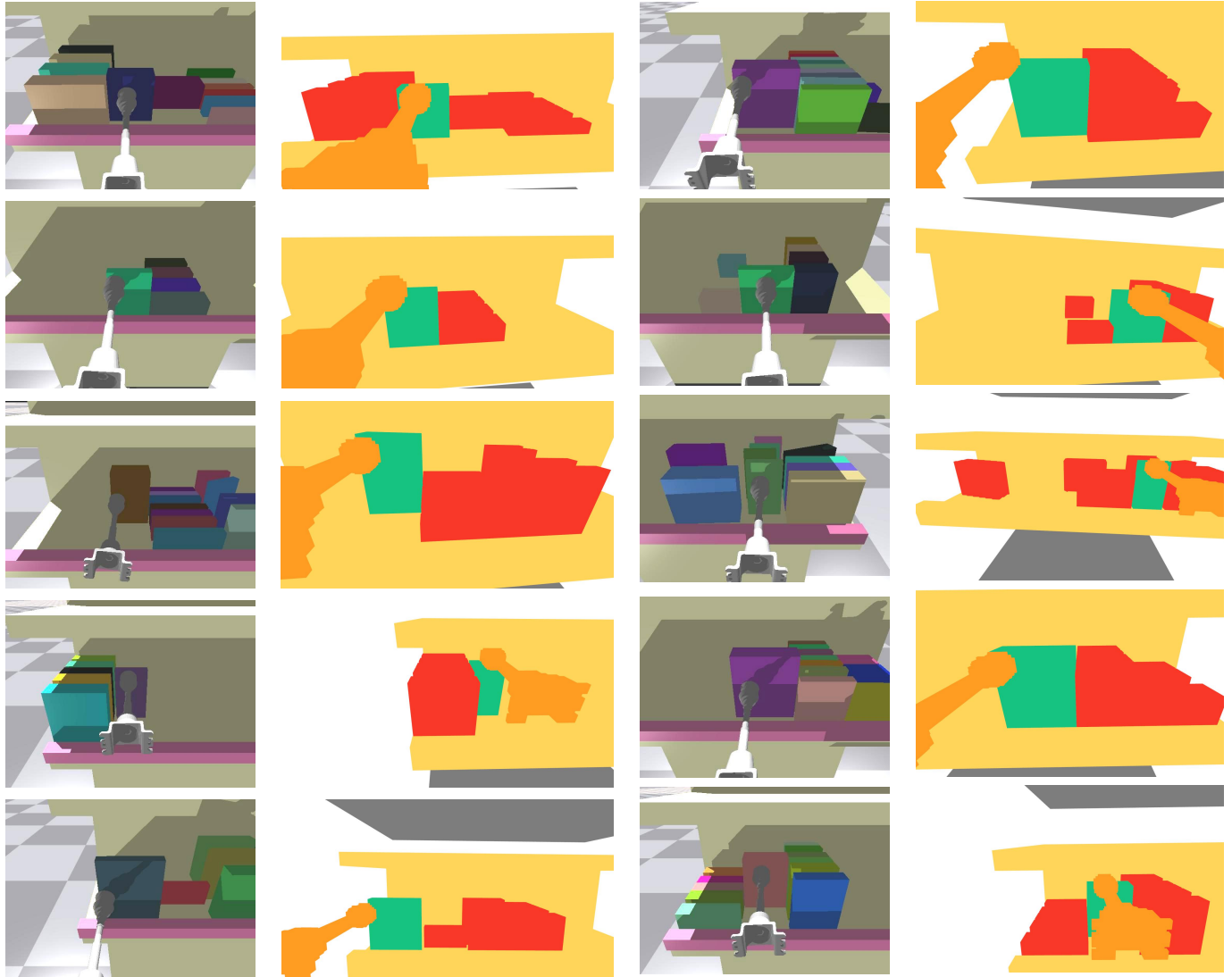


Fig. 6: Easy scenes, the first and third columns show the scenes in the simulation, while the second and fourth columns display the scenes generated by UniVoxGen.

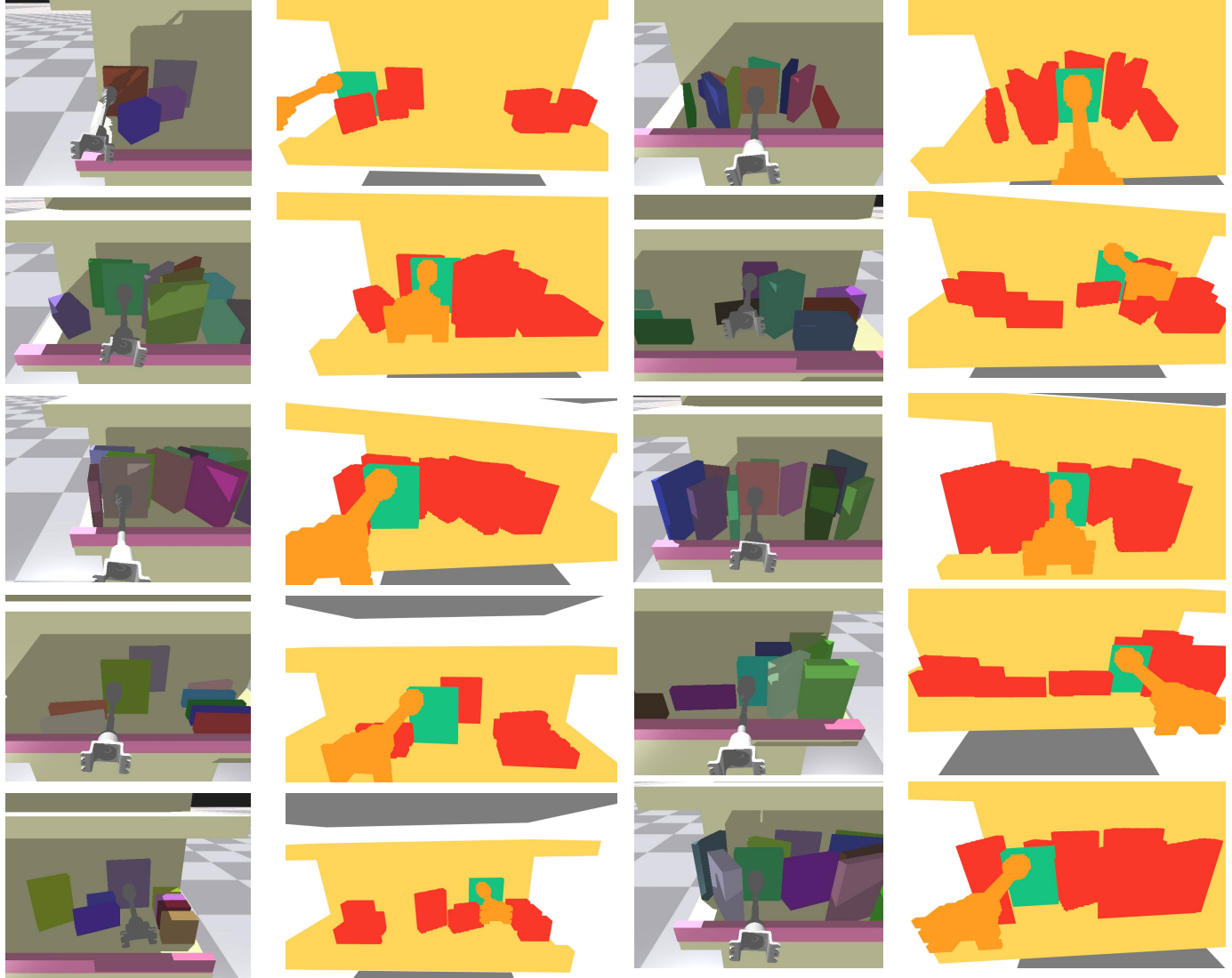


Fig. 7: Medium scenes, the first and third columns show the scenes in the simulation, while the second and fourth columns display the scenes generated by UniVoxGen.

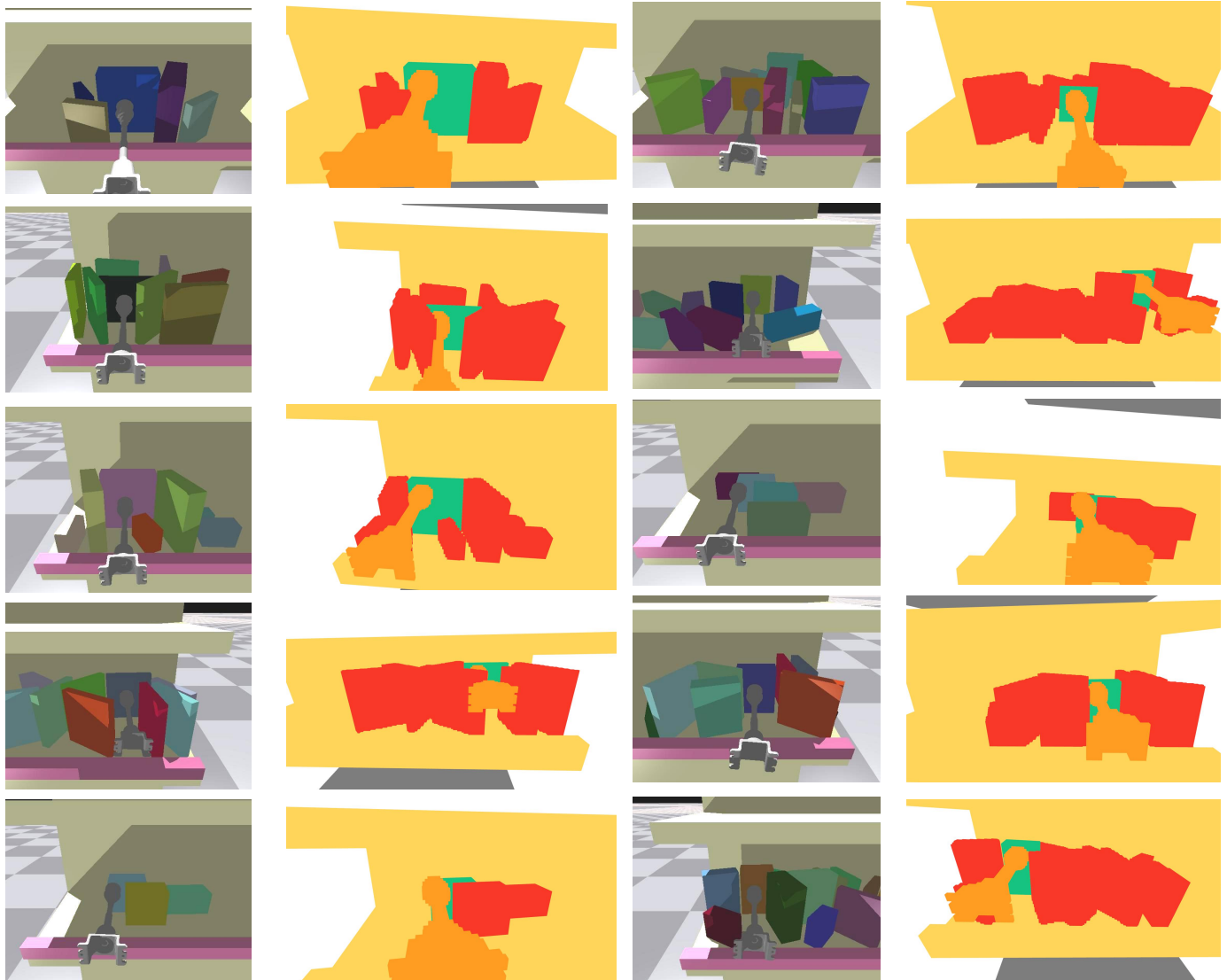


Fig. 8: Hard scenes, the first and third columns show the scenes in the simulation, while the second and fourth columns display the scenes generated by UniVoxGen.



Fig. 9: Items in Real-World Experiments